ACS OMEGA

http://pubs.acs.org/journal/acsodf

Article

DFT and Experimental Studies on the Mechanism of Mercury Adsorption on O_2-/NO-Codoped Porous Carbon

Hui Liu, Junyuan Li, Kaisong Xiang, Shudan He, and Fenghua Shen*

Cite This: *ACS Omega* 2021, 6, 12343−12350

Read Online

ACCESS | Metrics & More | Article Recommendations | Supporting Information

ABSTRACT: The utilization of O_2 and NO in flue gas to activate the raw porous carbon with auxiliary plasma contributes to an effective mercury (Hg)-removal strategy. The lack of in-depth knowledge on the Hg adsorption mechanism over the O_2-/NO-codoped porous carbon severely limits the development of a more effective Hg removal method and the potential application. Therefore, the generation processes of functional groups on the surface during plasma treatment were investigated and the detailed roles of different groups in Hg adsorption were clarified. The theoretical results suggest that the formation of functional groups is highly exothermic and they preferentially form on a carbon surface, and then affect Hg adsorption. The active groups affect Hg adsorption in a different manner, which depends on their nature. All of these active groups can improve Hg adsorption by enhancing the interaction of Hg with a surface carbon atom. Particularly, the preadsorbed NO_2 and O_3 groups can react directly with Hg by forming HgO. The experimental results confirm that the active groups cocontribute to the high Hg removal efficiency of O_2-/NO-codoped porous carbon. In addition, the mercury temperature-programmed desorption results suggest that there are two forms of mercury present on O_2-/NO-codoped porous carbon, including a carbon-bonded Hg atom and HgO.

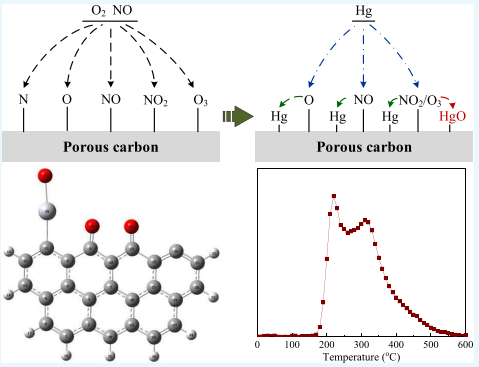

1. INTRODUCTION

Due to its persistence, bioaccumulation, and hypertoxicity, mercury (Hg) has attracted worldwide attention in environmental pollution management.[1−3] Minamata Convention on Mercury has thus been signed by 128 countries as an international effort to reduce the environmental contamination with Hg.[4−6] Fossil fuel utilization and nonferrous smelting are regarded as the main sources of anthropogenic pollution of Hg.[7−9] Therefore, Hg elimination from flue gases of coal combustion and nonferrous smelting has become a serious concern in mercury-emission control.

The removal of Hg using carbon materials as sorbents is one of the best Hg-emission control technologies.[10−12] The Hg-capture ability of carbon materials is closely related with their surface chemistry. To improve Hg-removal efficiency, active agents, such as oxygen, halogens, and sulfur, were often used to impregnate the carbon to create an additional active center.[13−15] However, such chemical impregnation methods are considered as time-consuming and not ecofriendly.[16−18] It is thus attractive to develop a simple, quick, and ecofriendly method to enhance the Hg-removal ability of carbon. In practical application, the Hg-removal performance of carbon has a close relationship with the flue gas component.[19−21] The effects of O_2 and NO on Hg removal by carbon were studied and it was suggested that O_2 and NO in flue gas could generate new surface-active groups, thereby facilitating Hg adsorption.[22] The previous findings indicate that if O_2 and NO present in flue gas can be utilized to enhance Hg adsorption, the cost of carbon activation will be significantly reduced and the pollutant NO will be removed as a cobenefit.

To achieve high Hg-removal efficiency, it is essential to enhance the positive effects of O_2 and NO on Hg adsorption, namely, enhancing the adsorption of O_2 and NO on carbon to create more active sites for Hg adsorption. In this aspect, nonthermal plasma coupled with porous carbon (PC) provides an achievable strategy.[23−25] High-energy electrons formed in plasma can excite O_2 and NO to generate energetic species, including N*, O*, NO*, NO_2*, O_3*, etc.[26−28] Such energetic species are more active to react with carbon than the gaseous molecules.[29] In addition, the porous carbon with a large surface area and a high pore volume offers fantastic opportunities to quickly and efficiently capture these energetic species.[30,31] Therefore, abundant active groups for Hg adsorption can be rapidly generated on a porous carbon surface by plasma. An effective strategy for Hg removal is thus established based on the combination of nonthermal plasma and porous carbon.

The Hg-removal ability of porous carbon is closely related to the functional groups generated by plasma. However, not all of

Received: March 15, 2021
Accepted: April 16, 2021
Published: April 27, 2021

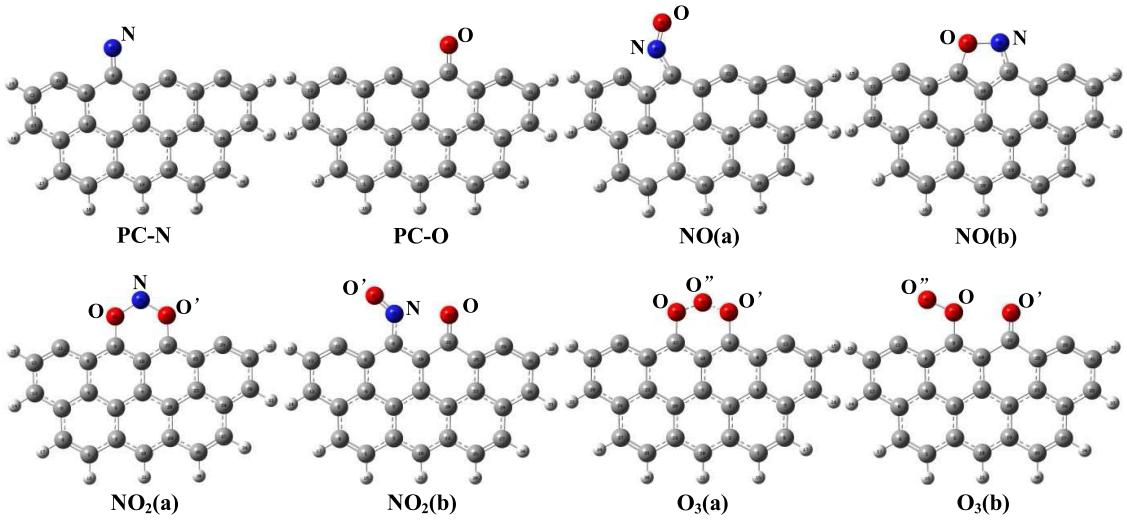

Figure 1. Optimized structures of reactive species adsorption on a porous carbon surface.

the functional groups are involved in Hg removal.[30,32,33] Therefore, to develop a more effective sorbent, it is important to elucidate the generation processes of functional groups on porous carbon, as well as their detailed roles in Hg removal. Nevertheless, the experimental method has some limitations in clarifying the functional group formation and Hg adsorption on a porous carbon surface because the microcosmic processes of energetic species and Hg adsorption are hard to be directly distinguished.[34] Fortunately, the density functional theory (DFT) method provides a powerful tool for understanding the adsorption mechanism at the molecular level.[35−37] However, no systematic theoretical study on the formation and evolution processes of functional groups on carbon during plasma treatment has been carried out. The detailed adsorption and oxidation processes of Hg on different types of groups remain to be explored.

In present work, the formation of different types of functional groups on porous carbon during plasma treatment under O_2 and NO was investigated by applying the density functional theory method. The detailed role of each type of group involved in Hg adsorption on carbon was identified. The pathways for Hg adsorption on porous carbon functionalized by plasma were proposed. Hg-removal experiments were conducted to study the contribution of different groups in Hg removal. This work provides molecular insight into the Hg removal by O_2- and NO-coadsorbed porous carbon, which helps to design a more effective method for simultaneously removing Hg and NO from flue gas.

2. RESULTS AND DISCUSSION

2.1. Adsorption of Energetic Species on a Porous Carbon Surface. The adsorption of energetic species generated by nonthermal plasma is the first step toward the formation of functional groups for Hg^0 adsorption on porous carbon. To reveal the generation and evolution processes of different functional groups, the adsorptions of N*, O*, NO*, NO_2*, and O_3* on different surface sites were examined, respectively. The most possible structures were optimized and are visualized in Figure 1.

The structure PC−N is formed by N* adsorption. The formation of PC−N is highly exothermic, with an exothermicity of −804.1 kJ/mol. Table S1 indicates the bond populations of PC−N, and the bond population of C−N in PC−N is 0.562. Such a high positive value of bond population suggests the formation of a strong covalent bond. In addition, there is an obvious decrease in the C−C bond populations where the N atom is directly involved, indicating that the strength of these C−C bonds is weakened to a greater extent as a result of N adsorption.

The structure PC−O is formed by O* adsorption on a carbon surface. The adsorption energy of O* in PC−O is found to be −946.0 kJ/mol, which means that O* adsorption is a highly exothermic process. As listed in Table S2, the C−O bond population of PC−O is 0.645, indicating a strong interaction of an O atom with a C atom.

Two stable configurations are obtained by NO* adsorption on a surface, including PC−NO(a) and PC−NO(b). PC−NO(a) represents the NO* approaching the carbon surface in a N-down mode, where the N atom is chemically bonded with the edge C atom. The adsorption energy of NO* in PC−NO(a) is −263.1 kJ/mol, and C−N bond population is 0.101 (Table S3). PC−NO(b) means NO* adsorbing in a side-on mode, where the N and O atoms are bonded with the edge C atom by forming a five-membered ring. The adsorption energy of NO* in PC−NO(b) is −571.6 kJ/mol, which is obviously larger than that of PC−NO(a). The bond populations of C−N and C−O are 0.377 and 0.204, respectively. The higher bond population confirms a stronger interaction of NO* with C atoms in PC−NO(b) than that in PC−NO(a). The results imply that NO* is more likely to be adsorbed with the N−O bond parallel to the edge.

The adsorption of NO_2* yields the stable structures PC−NO_2(a) and PC−NO_2(b). A six-membered ring is formed in PC−NO_2(a), where O and O′ atoms are bonded with C(9) and C(22), respectively. The bond population of C−O and C−O′ is 0.201 (Table S4), indicating a strong interaction of the O atom with the C site. However, both bond populations of N−O and N−O′ are only 0.079, which is obviously lower than the N−O bond population (0.246) in a gaseous NO_2 molecule. This means that the N−O bond is weakened after NO_2* adsorption. In PC−NO_2(b), NO_2* adsorbs dissociatively on the surface, where the two fragments NO′ and O atom adsorb on C(9) and C(22), respectively. The bond populations of C−N and C−O are 0.288 and 0.590, respectively, which are higher than the C−O bond population

https://doi.org/10.1021/acsomega.1c01391
ACS Omega 2021, 6, 12343−12350

in PC−NO_2(a), indicating a stronger interaction. The adsorption energy of NO_2* in PC−NO_2(b) is −529.3 kJ/mol, which is obviously higher than that in PC−NO_2(a) (−394.9 kJ/mol). This implies that NO_2* tends to adsorb on the surface in a dissociative manner.

The stable configurations PC−O_3(a) and PC−O_3(b) are derived from O_3* adsorption. In structure PC−O_3(a), a six-membered ring is formed between O_3* and edge C atoms. As listed in Table S5, both the bond populations of C−O and C−O′ are 0.213, indicating the formation of strong C−O bonds. However, both the O−O″ and O′−O″ bond populations are only 0.042, which is smaller than the O−O bond population (0.097) in a gaseous O_3 molecule. This suggests that the O−O bonds have been weakened after O_3* adsorption. In PC−O_3(b), O_3* dissociates into O−O″ and O′ atoms, and the two fragments adsorb on different C sites. Strong C−O bonds are formed in PC−O_3(b), as indicated by the positive bond populations. The adsorption energy of O_3* in PC−O_3(b) is found to be −768.2 kJ/mol, which is higher than that in PC−O_3(a) (−643.4 kJ/mol). This means that O_3* is likely to adsorb on the surface in a dissociative manner.

The above calculation results suggest that the adsorption of energetic species on porous carbon is a highly exothermic process. Various functional groups, including C−N, C−O_x, and C−NO_x, are formed on the surface after the plasma treatment under O_2 and NO, which is in consistence with the X-ray photoelectron spectroscopy (XPS) and Fourier transform infrared spectroscopy (FTIR) analyses.[29] Therefore, the improvement in the surface chemistry of porous carbon after plasma treatment can be assigned to the coadsorption of different energetic species.

2.2. Effects of Different Functional Groups on Hg Adsorption. *2.2.1. Hg Adsorption on Porous Carbon−N.* Hg adsorption on N*-preabsorbed carbon was studied, and two stable structures were obtained, including N−Hg(a) and N−Hg(b), as shown in Figure 2. The adsorption energies of Hg in

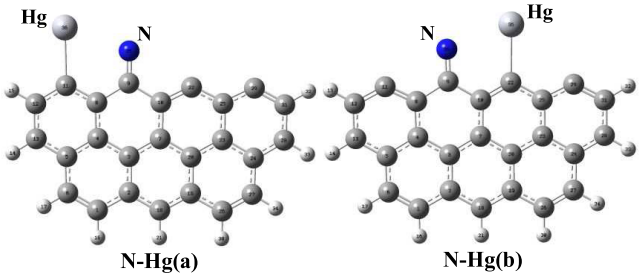

Figure 2. Hg adsorption on N-preadsorbed porous carbon.

N−Hg(a) and N−Hg(b) are −21.6 and −21.1 kJ/mol, respectively, and both are close to the Hg adsorption energy in PC−Hg (Figure S2, −17.8 kJ/mol). In addition, the C−Hg bond populations in N−Hg(a) and N−Hg(b) are 0.211 and 0.212 (Table S1), respectively, and both are also close to the C−Hg bond population (0.211) in PC−Hg. The calculation results reveal that a N group has a neglectable effect on the Hg adsorption on porous carbon.[23,38] The Hg removal using carbon was investigated experimentally. They increased the nitrogen groups on the carbon surface by applying nonthermal plasma treatment under pure N_2 and found that the nitrogen group had no obvious effect on the Hg removal ability of carbon. The calculation results are in agreement with the experimental phenomenon.

2.2.2. Hg Adsorption on Porous Carbon−O. The adsorption of Hg on O*-preabsorbed carbon was examined, and two stable configurations O−Hg(a) and O−Hg(b) were obtained, as illustrated in Figure 3. The Hg atom in these two

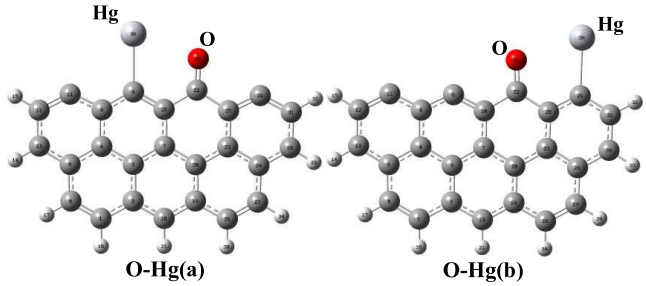

Figure 3. Hg adsorption on O-preadsorbed porous carbon.

structures is adsorbed on the edge C site rather than react directly with the O atom. The Hg adsorption energy is found to be −70.8 kJ/mol in O−Hg(a), and −57.9 kJ/mol in O−Hg(b). The Hg adsorption on PC−O is more exothermic than that on PC, confirming that the oxygen group can enhance the Hg^0-removal ability of porous carbon. The bond populations are listed in Table S2. It can be seen that the C−Hg bond populations in O−Hg(a) and O−Hg(b) are 0.229 and 0.222, respectively, and both are higher than the C−Hg bond population (0.211) in PC−Hg. This means that the oxygen group enhances Hg adsorption by improving the interaction of Hg with a C atom.

In previous experimental study,[30] the Hg-removal ability of oxygen-rich porous carbon was tested, and it was confirmed that an oxygen group could improve the Hg removal efficiency of porous carbon.[39] Various carbons were treated by air and nitric acid oxidation to increase the number of oxygen groups on the carbon surface. They found that increasing oxygen groups could improve the Hg-removal ability of carbon.[32] It was suggested experimentally that an oxygen group could enhance the electron-transfer process, and thus facilitating Hg adsorption on carbon. The calculation results are consistent with experimental conclusions.

2.2.3. Hg Adsorption on Porous Carbon−NO. The adsorption of Hg on a carbon surface with NO* was examined, and three stable intermediates NO−Hg(a), NO−Hg(b), and NO−Hg(c) were optimized, as shown in Figure 4, and the bond populations are indicated in Table S3. NO−Hg(a) represents the structure formed by Hg adsorption on PC−NO(a). The adsorption energy of Hg in NO−Hg(a) is only −2.8 kJ/mol, which is even lower than the Hg adsorption energy in PC−Hg (−17.8 kJ/mol). This means that when NO* is adsorbed on a surface in a N-down mode, it inhibits Hg adsorption. NO−Hg(b) and NO−Hg(c) means the Hg adsorption on PC−NO(b). The adsorption energies of Hg in NO−Hg(b) and NO−Hg(c) are −49.6 and −53.3 kJ/mol, respectively, which are more exothermic than Hg adsorption on PC. In addition, the C−Hg bond population in NO−Hg(b) and NO−Hg(c) is higher than that in PC−Hg. The results mean that the effect of NO* on Hg adsorption depends on the mode of NO* present on the surface. NO* can enhance Hg adsorption on the surface when it is adsorbed in a side-on mode, whereas it inhibits Hg adsorption when present in a N-down mode. Because NO* is more likely to adsorb in a side-on mode, NO* mainly plays a positive role in Hg adsorption. This

https://doi.org/10.1021/acsomega.1c01391
ACS Omega 2021, 6, 12343−12350

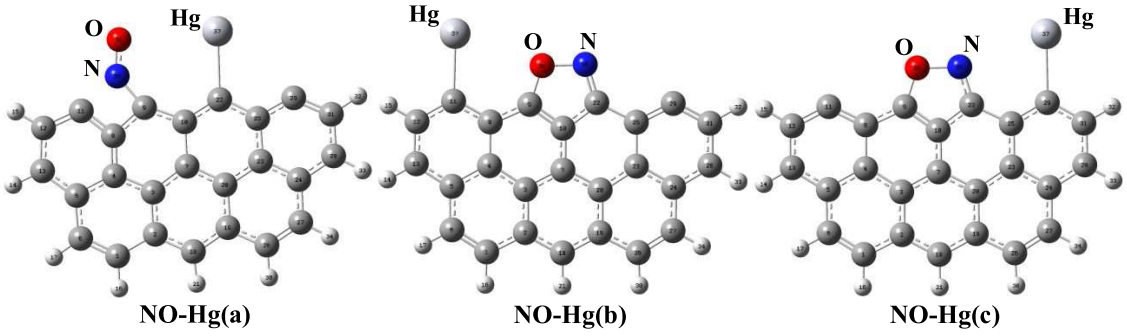

Figure 4. Hg adsorption on NO-preadsorbed porous carbon.

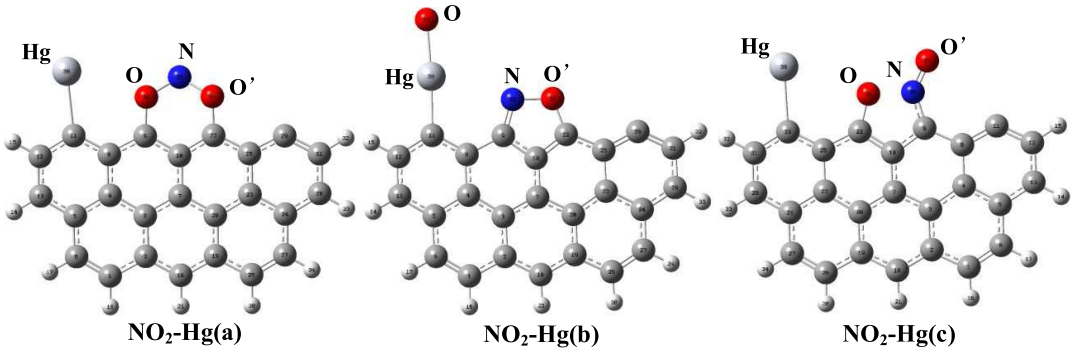

Figure 5. Hg adsorption on NO_2-preadsorbed porous carbon.

is consistent with the experimental phenomenon reported previously that NO could improve the Hg-removal ability of a carbon sorbent.[40]

2.2.4. Hg Adsorption on Porous Carbon−NO_2. Figure 5 illustrates the adsorption of Hg on a NO_2*-preadsorbed carbon surface, where three stable structures are obtained, including NO_2−Hg(a), NO_2−Hg(b), and NO_2−Hg(c). Among them, NO_2−Hg(a) and NO_2−Hg(b) are derived from Hg adsorbing on NO_2(a), and their formations are found to be exothermic with exothermicities of −39.6 and −124.4 kJ/mol, respectively. The bond population of C−Hg in NO_2−Hg(a) is 0.227, and is 0.366 in NO_2−Hg(b), lager than the C−Hg bond population of 0.211 in PC−Hg. Particularly, Hg is oxidized into HgO in NO_2−Hg(b), in which the Hg atom is bonded with a surface C atom. The adsorbed NO_2* decomposes into O and NO′, where the O atom is bonded with a Hg atom, and the remainder NO fragment bonds on C sites with a N−O bond parallel to the edge. The calculation result agrees well with the experimental one, suggesting that NO_2* on carbon can react with Hg by forming HgO and NO.[41] NO_2−Hg(c) is obtained from Hg adsorbing on PC−NO_2(b), in which the Hg adsorption energy is −48.8 kJ/mol. It is clear that Hg adsorption on a NO_2*-preadsorbed porous carbon surface is more exothermic than its adsorption on PC, confirming the positive effect of NO_2* on improving the Hg-removal ability of porous carbon. A similar conclusion was reached based on an experimental study using HNO_3-modified carbon to remove gaseous Hg.[42] The NO_2 group could facilitate Hg adsorption on a carbon surface.[43]

2.2.5. Hg Adsorption on Porous Carbon−O_3. The structures derived from Hg adsorption on a O_3*-preloaded carbon surface are presented in Figure 6, including O_3−Hg(a) and O_3−Hg(b). Among them, O_3−Hg(a) is originated from Hg adsorption on PC−O_3(a), and O_3−Hg(b) is calculated

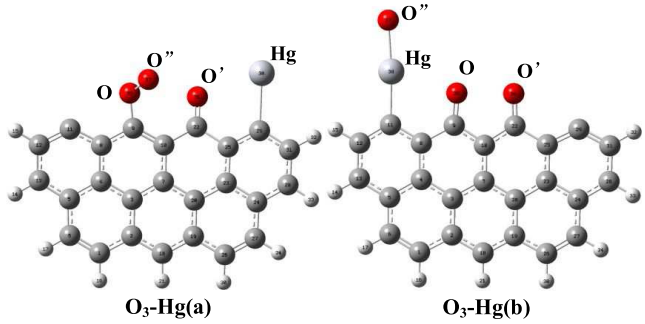

Figure 6. Hg adsorption on O_3-preadsorbed porous carbon.

from Hg on PC−O_3(b). The adsorption energy of Hg is −143.8 kJ/mol in O_3−Hg(a) and −143.2 kJ/mol in O_3−Hg(b). Particularly, HgO is formed in O_3−Hg(b), indicating that O_3* can oxidize Hg into HgO. The adsorption energy of Hg on carbon with O_3* is higher than that of Hg on PC, suggesting the positive effect of O_3* on Hg removal by porous carbon. In addition, Hg adsorption on O_3*-preadsorbed carbon is more exothermic than that on the other structures, indicating that O_3* is more effective in improving Hg removal.

2.3. Adsorption Pathway of Hg on Porous Carbon with Functional Groups. The calculation results indicate that the energetic species generated by plasma can be adsorbed on porous carbon with the formation of various surface functional groups. The formation processes of these groups are highly exothermic, and the exothermicities of these groups are significantly higher than the Hg adsorption. This means that the adsorption of energetic species is more stable than Hg. The energetic species will preferentially adsorb on carbon to form functional groups, which then affects the following Hg adsorption. As shown in Figure S4, the Mulliken charge of Hg in PC−Hg is lower than that in the other structures,

https://doi.org/10.1021/acsomega.1c01391
ACS Omega 2021, 6, 12343−12350

indicating an enhancement in charge transfer. The roles of different groups in Hg adsorption are closely related to their types. O*, NO*, NO_2*, and O_3* can generate active groups to enhance Hg adsorption, whereas N has no obvious effect on Hg removal.

To clarify the contribution of different groups in improving Hg adsorption on porous carbon, the Hg-removal abilities of PC, O_2−PC, NO−PC, and O_2/NO−PC were investigated, as shown in Figure 7. The average Hg removal efficiency of PC

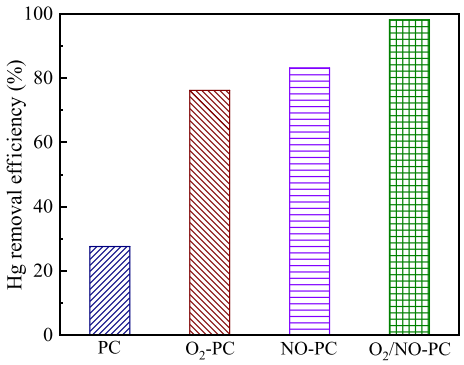

Figure 7. Hg removal efficiency of different porous carbons.

during 20 min test is only 27.6%, indicating a weak Hg-removal ability. After treated by the plasma under O_2, the average Hg-removal efficiency of O_2−PC increases to 76.2%, verifying the positive effect of the C−O_x group on Hg adsorption. The average Hg removal efficiency of NO−PC is found to be 83.2%, demonstrating the positive effect of C−NO_x on Hg adsorption. In addition, the average Hg removal efficiency of O_2/NO−PC is 98.2%, which is even higher than that of O_2−PC and NO−PC. This means that the excellent Hg-removal performance of O_2/NO−PC is owing to the coeffects of all active functional groups.

In addition, the mercury temperature-programmed desorption (Hg-TPD) method was applied to verify the forms of mercury on porous carbon. The Hg-preadsorbed raw PC and O_2/NO−PC were used for the desorption test, as shown in Figure 8. PC displays one Hg desorption peak at around 190 °C, which is assigned to the Hg directly adsorbed on carbon sites.[44,45] In contrast, O_2/NO−PC shows two distinguished Hg desorption peaks at 220 and 310 °C, respectively, demonstrating that there are two forms of mercury on the O_2/NO−PC surface. The first peak at 220 °C is contributed to

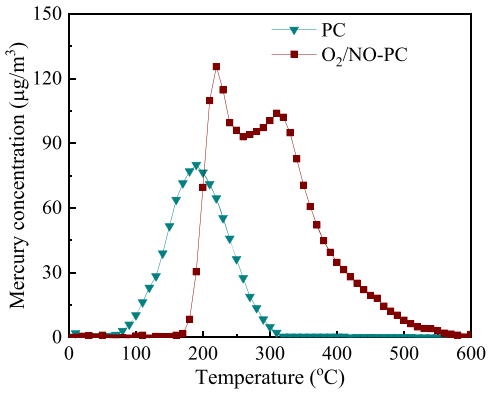

Figure 8. Hg-TPD profile of Hg-preadsorbed porous carbon.

Hg bonded with carbon sites, which occurs at a higher temperature than that of raw PC, confirming that the active functional groups can enhance the interaction of Hg with a C atom. The second peak at 310 °C is assigned to HgO,[44] which verifies that part of functional groups can oxidize Hg into HgO.

Based on the above theoretical and experimental investigations, the pathways for Hg adsorption on porous carbon treated by plasma under O_2 and NO can be obtained, as shown in Figure 9. On the one hand, the active functional groups do not react directly with Hg but can enhance the charge transfer between Hg and a surface C atom, thereby improving Hg adsorption on the neighboring C site. On the other hand, the preadsorbed NO_2* and O_3* can react directly with a Hg atom by forming HgO via the Eley−Rideal (ER) mechanism.

3. CONCLUSIONS

In this study, the generation processes of surface functional groups on porous carbon during plasma treatment under O_2 and NO were investigated, and the detailed roles of different groups in Hg adsorption were clarified. The surface functional groups are preferentially generated and then affect the following Hg adsorption. The effects of surface groups on Hg adsorption are closely related to their origin. The groups derived from O*, NO*, NO_2*, and O_3* adsorption can enhance Hg adsorption on a carbon surface, whereas the group formed by N adsorption has a neglectable effect on Hg adsorption. There are two pathways for functional groups enhancing Hg adsorption. One is that the active groups can improve Hg adsorption by enhancing the interaction of Hg with a surface carbon atom, and the other is that the preadsorbed NO_2* and O_3* can directly oxidize Hg into HgO via the Eley−Rideal mechanism. The high Hg-removal efficiency of the O_2-/NO-codoped porous carbon is assigned to the cocontribution of all active functional groups. The Hg-TPD method confirms that there are two forms of mercury present on a porous carbon surface, including Hg adsorbed on carbon sites and HgO adsorbed on the surface.

4. COMPUTATIONAL AND EXPERIMENTAL METHODS

4.1. Computational Details. In this study, the porous carbon acts as a reactant to capture the energetic species generated during plasma treatment and a gaseous Hg atom. It is thus important to choose a reasonable initial model for representing the structure of porous carbon. It is generally agreed that the macrostructure of carbon, including porous carbon, is mainly composed of polycyclic aromatic clusters of different sizes.[46,47] Solid-state ^{13}C NMR experiment confirms the chemical structure of carbon containing three to seven benzene rings.[48] Therefore, a seven benzene ring cluster model was applied to simulate the structure of porous carbon (PC), as shown in Figure S1. The edge unsaturated carbon atoms represent the main active sites on the carbon surface and the carbon atoms on the other sides are saturated by H atoms. Similar cluster models have been widely applied to represent the carbon structure for gaseous pollutant adsorption.[49,50]

Gaussian 16 software package was applied in this work.[51] Full geometry optimizations and frequency calculations were conducted for all of the structures using the B3PW91 functional. The 6-31G(d) basis set was employed for hydrogen, carbon, oxygen, and nitrogen atoms. The RCEP60VDZ basis set, with relativistic effective core potential

https://doi.org/10.1021/acsomega.1c01391
ACS Omega 2021, 6, 12343−12350

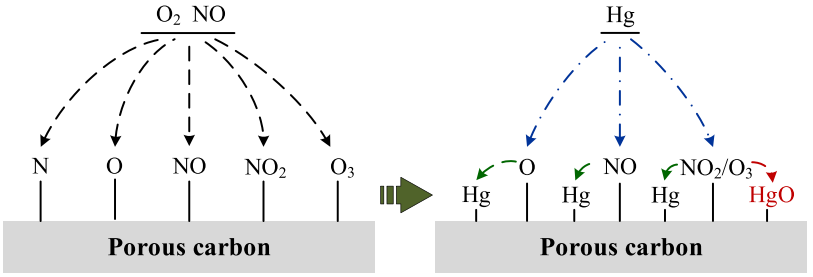

Figure 9. Illustrative profile of the proposed mechanism of Hg on different group surfaces.

(ECP), was used for a Hg atom, where the inner electrons were kept in the core. After the geometry optimizations and frequency calculations, the single-point energy calculations were performed using optimized structures by the def2-TZVP basis set, which was aimed to improve the accuracy of calculation results. To describe the weak interaction force of Hg adsorption, the density functional dispersion correction (DFT-D3) was adopted. Each structure was optimized at different multiplicities and the lowest energy complex was determined as a ground state. The method used to obtain adsorption energy is described in detail in the Supporting Information. The Mulliken method was adopted to investigate the charge-transfer process.

4.2. Experimental Justifications. To verify the calculation results, the Hg-removal efficiencies of different porous carbons were tested, including raw PC, PC treated by plasma under 4% O_2 (O_2−PC), PC treated by plasma under 200 ppm NO (NO−PC), and PC treated by plasma under 4% O_2 and 200 ppm NO (O_2/NO−PC). The mercury temperature-programmed desorption (Hg-TPD) method was used to investigate the forms of mercury present on a porous carbon surface. The samples were heated under pure N_2 at 10 °C/min from 20 to 600 °C. The gas flow rate was kept at 1.0 L/min. The experimental setup is showed in Figure S3. The experiments are described in detail in the Supporting Information.

■ ASSOCIATED CONTENT

Supporting Information

The Supporting Information is available free of charge at https://pubs.acs.org/doi/10.1021/acsomega.1c01391.

Sorbent preparation, nonthermal plasma treatment conditions, experimental system, Hg adsorption on raw carbon, and Mulliken atomic charges of Hg (PDF)

■ AUTHOR INFORMATION

Corresponding Author

Fenghua Shen − *School of Metallurgy and Environment, Central South University, Changsha 410083, China; Chinese National Engineering Research Center for Control & Treatment of Heavy Metal Pollution, Changsha 410083, China;* orcid.org/0000-0003-2522-2710; Phone: +86-731-88836804; Email: fhshen@csu.edu.cn; Fax: +86-731-88710171

Authors

Hui Liu − *School of Metallurgy and Environment, Central South University, Changsha 410083, China; Chinese National Engineering Research Center for Control & Treatment of Heavy Metal Pollution, Changsha 410083, China*

Junyuan Li − *School of Metallurgy and Environment, Central South University, Changsha 410083, China*

Kaisong Xiang − *School of Metallurgy and Environment, Central South University, Changsha 410083, China*

Shudan He − *School of Metallurgy and Environment, Central South University, Changsha 410083, China*

Complete contact information is available at: https://pubs.acs.org/10.1021/acsomega.1c01391

Notes

The authors declare no competing financial interest.

■ ACKNOWLEDGMENTS

This work was supported by the National Natural Science Foundation of China (51722407), the Science and Technology Project of Hunan Province (2019RS3006), and the Project of Innovation-driven Plan in Central South University (20180018050001).

■ REFERENCES

(1) Marcia, M. N. Mercury and Health. *Science* **2013**, *341*, No. 1430.
(2) Li, H.; Zhu, L.; Wang, J.; Li, L.; Shih, K. Development of nano-sulfide sorbent for efficient removal of elemental mercury from coal combustion fuel gas. *Environ. Sci. Technol.* **2016**, *50*, 9551−9557.
(3) Chen, L.; Liang, S.; Liu, M.; Yi, Y.; Mi, Z.; Zhang, Y.; Li, Y.; Qi, J.; Meng, J.; Tang, X.; Zhang, H.; Tong, Y.; Zhang, W.; Wang, X.; Shu, J.; Yang, Z. Trans-provincial health impacts of atmospheric mercury emissions in China. *Nat. Commun.* **2019**, *10*, No. 1484.
(4) Eyrikh, S.; Eichler, A.; Tobler, L.; Malygina, N.; Papina, T.; Schwikowski, M. A 320 year ice-core record of atmospheric Hg pollution in the Altai, Central Asia. *Environ. Sci. Technol.* **2017**, *51*, 11597−11606.
(5) Shen, F.; Liu, J.; Wu, D.; Gu, C.; Dong, Y. Molecular-level insights into effect mechanism of H_2S on mercury removal by activated carbon. *Ind. Eng. Chem. Res.* **2018**, *57*, 7889−7897.
(6) Xiao, Y.; Pudasainee, D.; Gupta, R.; Xu, Z.; Diao, Y. Bromination of petroleum coke for elemental mercury capture. *J. Hazard. Mater.* **2017**, *336*, 232−239.
(7) Lee, S. S.; Wilcox, J. Behavior of mercury emitted from the combustion of coal and dried sewage sludge: The effect of unburned carbon, Cl, Cu and Fe. *Fuel* **2017**, *203*, 749−756.
(8) Wu, Q.; Li, G.; Wang, S.; Liu, K.; Hao, J. Mitigation options of atmospheric Hg emissions in China. *Environ. Sci. Technol.* **2018**, *52*, 12368−12375.
(9) Yang, S.; Liu, C.; Wang, P.; Yi, H.; Shen, F.; Liu, H. Co_9S_8 nanoparticles-embedded porous carbon: a highly efficient sorbent for mercury capture from nonferrous smelting flue gas. *J. Hazard. Mater.* **2021**, *412*, No. 124970.
(10) Graydon, J. W.; Zhang, X.; Kirk, D. W.; Jia, C. Q. Sorption and stability of mercury on activated carbon for emission control. *J. Hazard. Mater.* **2009**, *168*, 978−982.

(11) Yang, Y.; Liu, J.; Zhang, B.; Liu, F. Mechanistic studies of mercury adsorption and oxidation by oxygen over spinel-type $MnFe_2O_4$. *J. Hazard. Mater.* **2017**, *321*, 154−161.
(12) Shen, F.; Liu, J.; Dong, Y.; Wu, D. Mercury removal by biomass-derived porous carbon: Experimental and theoretical insights into the effect of H_2S. *Chem. Eng. J.* **2018**, *348*, 409−415.
(13) Hsi, H. C.; Tsai, C. Y.; Kuo, T. H.; Chiang, C. S. Development of low-concentration mercury adsorbents from biohydrogen-generation agricultural residues using sulfur impregnation. *Bioresour. Technol.* **2011**, *102*, 7470−7477.
(14) Li, G.; Shen, B.; Li, F.; Tian, L.; Singh, S.; Wang, F. Elemental mercury removal using biochar pyrolyzed from municipal solid waste. *Fuel Process. Technol.* **2015**, *133*, 43−50.
(15) Li, H.; Zhu, L.; Wang, J.; Li, L.; Lee, P. H.; Feng, Y.; Shih, K. Effect of nitrogen oxides on elemental mercury removal by nanosized mineral sulfide. *Environ. Sci. Technol.* **2017**, *51*, 8530−8536.
(16) Li, G.; Wang, S.; Wu, Q.; Wang, F.; Shen, B. Mercury sorption study of halides modified bio-chars derived from cotton straw. *Chem. Eng. J.* **2016**, *302*, 305−313.
(17) Ambrosy, J. M.; Pasel, C.; Luckas, M.; Bittig, M.; Bathen, D. A detailed investigation of adsorption isotherms, enthalpies, and kinetics of mercury adsorption on nonimpregnated activated carbon. *Ind. Eng. Chem. Res.* **2019**, *58*, 4208−4221.
(18) Zhang, K.; Min, X.; Zhang, T.; Si, M.; Jiang, J.; Chai, L.; Shi, Y. Biodeposited nano-CdS drives the In situ growth of highly dispersed sulfide nanoparticles during pyrolysis for enhanced oxygen evolution reaction. *ACS Appl. Mater. Interfaces* **2020**, *12*, 54553−54562.
(19) Presto, A. A.; Granite, E. J. Impact of sulfur oxides on mercury capture by activated carbon. *Environ. Sci. Technol.* **2007**, *41*, 6579−6584.
(20) Gao, L.; Li, C.; Zhang, J.; Du, X.; Li, S.; Zeng, J.; Yi, Y.; Zeng, G. Simultaneous removal of NO and Hg^0 from simulated flue gas over CoO_x-CeO_2 loaded biomass activated carbon derived from maize straw at low temperatures. *Chem. Eng. J.* **2018**, *342*, 339−349.
(21) Li, G.; Wu, Q.; Wang, S.; Li, Z.; Liang, H.; Tang, Y.; Zhao, M.; Chen, L.; Liu, K.; Wang, F. The influence of flue gas components and activated carbon injection on mercury capture of municipal solid waste incineration in China. *Chem. Eng. J.* **2017**, *326*, 561−569.
(22) Li, Y.; Duan, Y.; Wang, H.; Zhao, S.; Chen, M.; Liu, M.; Wei, H. Effects of acidic gases on mercury adsorption by activated carbon in simulated oxy-fuel combustion flue gas. *Energy Fuels* **2017**, *31*, 9745−9751.
(23) Zhang, B.; Xu, P.; Qiu, Y.; Yu, Q.; Ma, J.; Wu, H.; Luo, G.; Xu, M.; Yao, H. Increasing oxygen functional groups of activated carbon with non-thermal plasma to enhance mercury removal efficiency for flue gases. *Chem. Eng. J.* **2015**, *263*, 1−8.
(24) Shen, F.; Liu, J.; Wu, D.; Dong, Y.; Liu, F.; Huang, H. Design of O_2/SO_2 dual-doped porous carbon as superior sorbent for elemental mercury removal from flue gas. *J. Hazard. Mater.* **2019**, *366*, 321−328.
(25) Shi, M.; Luo, G.; Xu, Y.; Zou, R.; Zhu, H.; Hu, J.; Li, X.; Yao, H. Using H_2S plasma to modify activated carbon for elemental mercury removal. *Fuel* **2019**, *254*, No. 115549.
(26) Wang, T.; Sun, B. Effect of temperature and relative humidity on NO_x removal by dielectric barrier discharge with acetylene. *Fuel Process. Technol.* **2016**, *144*, 109−114.
(27) Zhang, J.; Duan, Y.; Zhou, Q.; Zhu, C.; She, M.; Ding, W. Adsorptive removal of gas-phase mercury by oxygen non-thermal plasma modified activated carbon. *Chem. Eng. J.* **2016**, *294*, 281−289.
(28) Wang, Z.; Jiang, S.; Zhu, Y.; Zhou, J.; Zhou, J.; Li, Z.; Cen, K. Investigation on elemental mercury oxidation mechanism by non-thermal plasma treatment. *Fuel Process. Technol.* **2010**, *91*, 1395−1400.
(29) Shen, F.; Liu, J.; Wu, D.; Dong, Y.; Zhang, Z. Development of O_2 and NO co-doped porous carbon as a high-capacity mercury sorbent. *Environ. Sci. Technol.* **2019**, *53*, 1725−1731.
(30) Shen, F.; Liu, J.; Zhang, Z.; Dong, Y.; Yang, Y.; Wu, D. Oxygen-rich porous carbon derived from biomass for mercury removal: An experimental and theoretical study. *Langmuir* **2018**, *34*, 12049−12057.
(31) Zheng, C.; Yang, Z.; Si, M.; Zhu, F.; Yang, W.; Zhao, F.; Shi, Y. Application of biochars in the remediation of chromium contamination: Fabrication, mechanisms, and interfering species. *J. Hazard. Mater.* **2021**, *407*, No. 124376.
(32) Tan, Z.; Sun, L.; Xiang, J.; Zeng, H.; Liu, Z.; Hu, S.; Qiu, J. Gas-phase elemental mercury removal by novel carbon-based sorbents. *Carbon* **2012**, *50*, 362−371.
(33) Zheng, J. M.; Shah, K. J.; Zhou, J. S.; Pan, S. Y.; Chiang, P. C. Impact of HCl and O_2 on removal of elemental mercury by heat-treated activated carbon: Integrated X-ray analysis. *Fuel Process. Technol.* **2017**, *167*, 11−17.
(34) Wang, Z.; Liu, J.; Yang, Y.; Liu, F.; Ding, J. Heterogeneous reaction mechanism of elemental mercury oxidation by oxygen species over MnO_2 catalyst. *Proc. Combust. Inst.* **2019**, *37*, 2967−2975.
(35) Zhang, Z.; Zhou, C.; Wu, H.; Liu, J.; Yang, H. Molecular study of heterogeneous mercury conversion mechanism over Cu-MOFs: Oxidation pathway and effect of halogen. *Fuel* **2021**, *290*, No. 120030.
(36) Jiao, A.; Jiang, X.; Liu, J.; Ma, Y.; Zhang, H. Density functional theory investigation on the catalytic reduction of NO by CO on the char surface: the effect of Iron. *Environ. Sci. Technol.* **2020**, *54*, 2422−2428.
(37) He, P.; Zhang, Y.; Zhao, X.; Wei, J.; Xu, T.; Wu, J.; Chen, N. Effect of flue gas on elemental mercury removal capacity of defective carbonaceous surface: A first-principles study. *J. Hazard. Mater.* **2020**, *404*, No. 124013.
(38) Zhang, B.; Zeng, X.; Xu, P.; Chen, J.; Xu, Y.; Luo, G.; Xu, M.; Yao, H. Using the novel method of nonthermal plasma to add Cl active sites on activated carbon for removal of mercury from flue gas. *Environ. Sci. Technol.* **2016**, *50*, 11837−11843.
(39) Li, Y. H.; Lee, C. W.; Gullett, B. K. Importance of activated carbon's oxygen surface functional groups on elemental mercury adsorption. *Fuel* **2003**, *82*, 451−457.
(40) Yang, W.; Li, Y.; Shi, S.; Chen, H.; Shan, Y.; Liu, Y. Mercury removal from flue gas by magnetic iron-copper oxide modified porous char derived from biomass materials. *Fuel* **2019**, *256*, No. 115977.
(41) Tan, Z.; Xiang, J.; Su, S.; Zeng, H.; Zhou, C.; Sun, L.; Hu, S.; Qiu, J. Enhanced capture of elemental mercury by bamboo-based sorbents. *J. Hazard. Mater.* **2012**, *239*−*240*, 160−166.
(42) Tong, L.; Xu, W.; Zhou, X.; Liu, R.; Zhu, T. Effects of multi-component flue gases on Hg^0 removal over HNO_3-modified activated carbon. *Energy Fuels* **2015**, *29*, 5231−5236.
(43) Tong, L.; Yue, T.; Zuo, P.; Zhang, X.; Wang, C.; Gao, J.; Wang, K. Effect of characteristics of KI-impregnated activated carbon and flue gas components on Hg^0 removal. *Fuel* **2017**, *197*, 1−7.
(44) Rumayor, M.; Lopez-Anton, M. A.; Díaz-Somoano, M.; Martínez-Tarazona, M. R. A new approach to mercury speciation in solids using a thermal desorption technique. *Fuel* **2015**, *160*, 525−530.
(45) Sun, P.; Zhang, B.; Zeng, X.; Luo, G.; Li, X.; Yao, H.; Zheng, C. Deep study on effects of activated carbon's oxygen functional groups for elemental mercury adsorption using temperature programmed desorption method. *Fuel* **2017**, *200*, 100−106.
(46) Smith, M. W.; Dallmeyer, I.; Johnson, T. J.; Brauer, C. S.; McEwen, J.-S.; Espinal, J. F.; Garcia-Perez, M. Structural analysis of char by Raman spectroscopy: Improving band assignments through computational calculations from first principles. *Carbon* **2016**, *100*, 678−692.
(47) Montoya, A.; Truong, T. N.; Sarofim, A. F. Application of density functional theory to the study of the reaction of NO with char-bound nitrogen during combustion. *J. Phys. Chem. A* **2000**, *104*, 8409−8417.
(48) Perry, S.; Hambly, E.; Fletcher, T.; Solum, M.; Pugmire, R. Solid-state 13C NMR characterization of matched tars and chars from rapid coal devolatilization. *Proc. Combust. Inst.* **2000**, *28*, 2313−2319.
(49) Liu, J.; Qu, W.; Zheng, C. Theoretical studies of mercury−bromine species adsorption mechanism on carbonaceous surface. *Proc. Combust. Inst.* **2013**, *34*, 2811−2819.
(50) Liu, J.; Qu, W.; Joo, S. W.; Zheng, C. Effect of SO_2 on mercury binding on carbonaceous surfaces. *Chem. Eng. J.* **2012**, *184*, 163−167.

https://doi.org/10.1021/acsomega.1c01391
ACS Omega 2021, 6, 12343−12350

(51) Frisch, M. J.; Trucks, G. W.; Schlegel, H. B.; Scuseria, G. E.; Robb, M. A.; Cheeseman, J. R.; Scalmani, G.; Barone, V.; Petersson, G. A.; Nakatsuji, H.; Li, X.; Caricato, M.; Marenich, A. V.; Bloino, J.; Janesko, B. G.; Gomperts, R.; Mennucci, B.; Hratchian, H. P.; Ortiz, J. V.; Izmaylov, A. F.; Sonnenberg, J. L.; Williams; Ding, F.; Lipparini, F.; Egidi, F.; Goings, J.; Peng, B.; Petrone, A.; Henderson, T.; Ranasinghe, D.; Zakrzewski, V. G.; Gao, J.; Rega, N.; Zheng, G.; Liang, W.; Hada, M.; Ehara, M.; Toyota, K.; Fukuda, R.; Hasegawa, J.; Ishida, M.; Nakajima, T.; Honda, Y.; Kitao, O.; Nakai, H.; Vreven, T.; Throssell, K.; Montgomery, J. A., Jr.; Peralta, J. E.; Ogliaro, F.; Bearpark, M. J.; Heyd, J. J.; Brothers, E. N.; Kudin, K. N.; Staroverov, V. N.; Keith, T. A.; Kobayashi, R.; Normand, J.; Raghavachari, K.; Rendell, A. P.; Burant, J. C.; Iyengar, S. S.; Tomasi, J.; Cossi, M.; Millam, J. M.; Klene, M.; Adamo, C.; Cammi, R.; Ochterski, J. W.; Martin, R. L.; Morokuma, K.; Farkas, O.; Foresman, J. B.; Fox, D. J.; et al. *Gaussian 16*, revision B.01; Gaussian Inc.: Wallingford, CT, 2016.

https://doi.org/10.1021/acsomega.1c01391
ACS Omega 2021, 6, 12343−12350